Japanese Journal of Applied Physics **50** (2011) 070117
DOI: 10.1143/JJAP.50.070117

Characteristics of p–i–n Terahertz and Infrared Photodiodes Based on Multiple Graphene Layer Structures

Maxim Ryzhii[1,3], Taiichi Otsuji[2,3], Vladimir Mitin[4], and Victor Ryzhii[1,3]

[1] *Computational Nanoelectronics Laboratory, University of Aizu, Aizuwakamatsu, Fukushima 965-8580, Japan*
[2] *Research Institute for Electrical Communication, Tohoku University, Sendai 980-8577, Japan*
[3] *Japan Science and Technology Agency, CREST, Chiyoda, Tokyo 107-0075, Japan*
[4] *Department of Electrical Engineering, University at Buffalo, Buffalo, NY 1460-1920, U.S.A.*

Received November 30, 2010; accepted February 4, 2011; published online July 20, 2011

We calculate the responsivity and dark-current-limited detectivity of terahertz and infrared interband detectors based on p–i–n junctions in the multiple graphene layer structures proposed recently. It is demonstrated that the interband tunneling can be an essential limiting mechanism of the ultimate values of detectivity. To achieve the ultimate detectivity, the optimization of the device structure and the proper choice of the temperature and the bias voltage are required. We show that owing to high values of the quantum efficiency and relatively low rates of thermogeneration, the detectors under consideration can exhibit high responsivity and detectivity at elevated temperatures (in particular, at room temperature) in a wide radiation spectrum and can substantially surpass other detectors.

1. Introduction

The carbon-based materials promise many interesting device applications. These materials include different crystal forms: diamond, graphite, fullerenes, and carbon nanotubes. Recently, this series has been extended by graphene, a monolayer of carbon atoms forming a dense honeycomb two-dimensional crystal structure. Among other unique features, graphene layers (GLs) exhibit very specific optical properties associated with the gapless energy spectrum and the linear dispersion law for electrons and holes (see, for instance, an extensive review by Castro Neto *et al.*[1]). A rather high quantum efficiency of interband transitions in a single GL[2,3] enables the use of GLs, as well as graphene bilayers (GBLs) and graphene nanoribbons (GNRs), for high-performance sources (in particular, lasers) and detectors of terahertz (THz) and infrared (IR) radiation (see, for instance, refs. 4–10). As discovered recently (see the paper by Sprinkle *et al.*[11] as well as the review paper by Orlita and Potemski[12] and the references therein), the stacks of disoriented non-Bernal stacked GLs epitaxially grown on a C-terminated surface of 4H-SiC, which were called by the authors the multiple epitaxial graphene (MEG) exhibit virtually the same electron and optical properties as individual GLs. This is in contrast to the GL structures with Bernal stacking, because the rotational stacking causes GLs to electronically decouple, which leads to a set of nearly independent energy bands with the linear dispersion for electrons and holes.[11] Due to the contributions of each GL to the optical absorption, the system of such GLs can exhibit a fairly high absorption coefficient. Such a system of a multiple-GL (MGL) structure can be considered as a new form of carbon[11] that can be a novel material for optoelectronics. One of the remarkable features of this material is the high quality of GLs, which are characterized by fairly long electron and hole momentum relaxation times. The latter provides a relatively low intraband (Drude) absorption of radiation. To distinguish the MGL structures under consideration (or the MEG structures) from graphite and the multiple-layer structures with Bernal staking, for example, grown on the Si face of 4H-SIC or 6H-SiC, one could introduce a special term for this material (e.g., "grapheneplex" instead of MEG). A variety of planar carbon structures are shown in Fig. 1. The use of grapheneplex opens up the prospect of farther enhancement of graphene-based optoelectronic devices.[13–15] THz and IR detectors based on multiple GL structures with either chemically doped or electrically induced p–i–n junctions have recently been proposed and evaluated.[15] These detectors, which are referred to as multiple-GL photodiodes (MGL-PDs) below, are shown in Figs. 2(a) and 2(b), where V is the bias voltage.

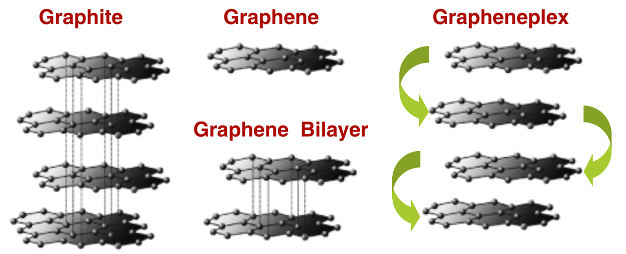

Fig. 1. (Color online) Schematic view of planar carbon structures with different numbers of GLs.

In this study, we investigate the MGL-PDs using a simplified device model[15] focusing our consideration on their ultimate performance. In particular, we calculate the MGL-PD responsivity and dark-current-limited detectivity, which are the main detector characteristics.[16] As expected previously[15] and shown in the present paper, the interband tunneling, resulting in a marked dark current, can substantially limit the MGL-PD detectivity at lowered temperatures.

The formation of chemically doped lateral p–i–n junctions of GLs was realized by Avouris and his co-workers.[17] The doped p–i–n junctions and electrically induced p–i–n junctions[18] (see also refs. 15 and 19) in gated GL structures are shown in Figs. 2(a) and 2(b), respectively. The treatments of GL-PDs with chemical and electrical doping are similar, although in the case of the latter, an extra complexity can arise.[15,19] For definiteness, we primarily restrict our present study to MGL-PDs with chemically formed p–i–n junctions. As demonstrated, the MGL-PDs can exhibit fairly high responsivity and dark-current limited detectivity. This is mainly due to the high values of quantum efficiency and the low rate of electron and hole thermo-

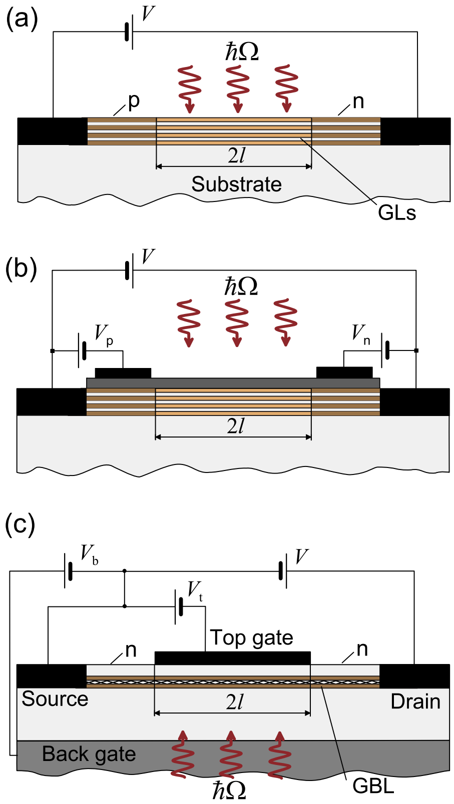

Fig. 2. (Color online) Schematic views of (a) MGL-PD with chemically doped p- and n-sections, (b) MGL-PD with electrical doping, and (c) GBL-PT (V_n and V_p are the gate voltages that induce the pertinent electron and hole charges beneath the gates).

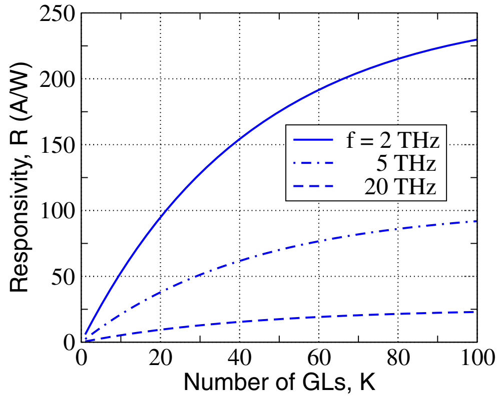

Fig. 3. (Color online) MGL-PD responsivity as a function of number of GLs for different radiation frequencies.

generation. However, the MGL-PD photoelectric gain is approximately or less than unity. We compare the responsivity and detectivity of MGL-PDs with those of the field-effect phototransistors with the GBL channel (GBL-FETs). The GBL-FET phototransistor structure (for which we shall use the abbreviation GBL-PT) is shown in Fig. 2(c). In contrast, the GBL-FETs exhibit moderate quantum efficiency but rather high photoelectric gain.[10)]

2. MGL-PD Responsivity

We consider MGL-PDs with the structure shown in Fig. 2(a), assuming that the p–i–n junction is reverse-biased (bias voltage $V < 0$). The current (per unit width perpendicular to its direction) created in the MGL-PD by photogenerated electrons and holes, i.e., the photocurrent, can be calculated using the following formula:

$$J_{\text{photo}} = \frac{4le[1-(1-\beta_\Omega)^K)]}{\hbar\Omega} Ig. \qquad (1)$$

Here, e is the electron charge, $2l$ is the length of the i-sections (see Fig. 1), $\hbar$ is the reduced Planck constant, K is the number of GLs, β_Ω is the interband absorption coefficient of radiation, and I is the power density of incident radiation. The latter is given by the Falkovski–Varlamov formula[2)] $\beta_\Omega = \beta[1 - 2F(\hbar\Omega/2)] \simeq \beta$, where $\beta = \pi e^2/c\hbar \simeq \pi/137 \simeq 0.023$, c is the speed of light in vacuum, and $F(\varepsilon)$ (for the conditions under consideration, $F(\hbar\Omega/2) \ll 1$) is the electron (hole) energy distribution function in the i-sections of each GL. The factor g is the photoelectric gain. If the length of the i-section $2l$ is sufficiently small such that the electron and hole transit time across this section is shorter than the chracteristic recombination time τ_r, all the photogenerated electrons and holes are managed to contribute to the photocurrent during their propagation across the i-section. In this case, $g \simeq 1$. In the MGL-PDs with relatively long i-sections, the recombination of the photogenerated electrons and holes decreases their contribution to the photocurrent, so that $g < 1$. Equation (1) accounts for the dependence of the photogeneration rate on the GL index (due to the attenuation of radiation associated with its absorption in the GLs located closer to the structure top). Using eq. (1), the MGL-PD responsivity $R = J_{\text{photo}}/2lI$ can be presented as

$$R = \frac{2eg[1-(1-\beta)^K]}{\hbar\Omega}. \qquad (2)$$

Introducing the effective number of GLs $K^* = [1 - (1-\beta)^K)]/\beta < K$ and the quantum efficiency $\eta = 2[1 - (1-\beta)^K)] = 2\beta K^*$, the MGL-PD responsivity can be presented in the standard form:

$$R = K^* \frac{2eg\beta}{\hbar\Omega} = \frac{eg\eta}{\hbar\Omega}. \qquad (3)$$

In an MGL-PD with $K = 1$, $\eta \simeq 0.046$. If $K = 100$, one obtains $K^* = 39$, and $\eta \simeq 1.80$. The quantity η can exceed unity because one absorbed photon generates two particles: an electron and a hole.

The dependences of the MGL-PD responsivity R on the number of GLs, K, calculated for different radiation frequencies $f = \Omega/2\pi$ are shown in Fig. 3. One can see that the responsivity of MGL-PDs increases sublinearly with increasing number of GLs. This is natural because the quantum efficiency η rises when K, and consequently K^*, increases. As follows from Fig. 3, at a sufficiently large number of GLs, the MGL-PD responsivity is very high in a fairly wide range of radiation frequencies. This is attributed to a strong interband absorption (in each of the multiple GLs) and almost flat its spectral dependence.

3. MGL-PD Detectivity

The dark-current-limited detectivity D^* is usually defined as $D^* = (J_{\text{photo}}/NP \cdot \Delta f^{1/2})$, where $P = 2lHI$ is the power received by the photodetector, $2lH$ and H are respectively the device area and width in the direction perpendicular to the current, Δf is the bandwidth, and N is the noise.[20] The noise can be expressed via the dark current $J_{\rm dark}$, as $N = (4eg_{\rm noise}J_{\rm dark}H\Delta f)^{1/2}$, where $g_{\rm noise}$ is the noise gain. The dark current, which comprises the component associated with the interband thermogeneration and tunneling generation of electrons and holes in the i-section, is given by

$$J_{\rm dark} = 4Kel(G_{\rm th} + G_{\rm tunn}), \tag{4}$$

where $G_{\rm th}$ and $G_{\rm tunn}$ are the thermogeneration and tunneling rates in each GL per unit of its area.

Expressing the noise via the dark current, using eq. (3), and setting $g = g_{\rm noise} = 1$, we obtain

$$D^* = \frac{K^*\beta}{\hbar\Omega\sqrt{2K(G_{\rm th} + G_{\rm tunn})}}. \tag{5}$$

At not too low temperatures, the interband thermogeneration is primarily associated with the absorption of optical phonons.[21] Considering that the number of optical phonons at the temperature $T \ll \hbar\omega_0/k_{\rm B}$ is equal to $\mathcal{N}_0 \simeq \exp(-\hbar\omega_0/k_{\rm B}T)$, where $\hbar\omega \simeq 0.2\,{\rm eV}$ is the optical phonon energy and $k_{\rm B}$ is the Boltzmann constant, we shall use the following simplified formula:

$$G_{\rm th} = \overline{G_{\rm th}}\exp\left(-\frac{\hbar\omega_0}{k_{\rm B}T}\right), \tag{6}$$

where $\overline{G_{\rm th}}$ is a pre-exponential factor, which, for simplicity, is assumed to be independent of the temperature. Comparing eq. (7) with the results of numerical calculations,[19] we set $\overline{G_{\rm th}} = 3\times 10^{24}\,{\rm cm^{-2}\,s^{-1}}$, so that at $T = 300\,{\rm K}$, one obtains $G_{\rm th} \sim 10^{21}\,{\rm cm^{-2}\,s^{-1}}$.

The interband tunneling rate in a GL at the electric field $\mathcal{E} = V/2l$ is given by[7]

$$G_{\rm tunn} = \frac{1}{4\pi\, v_{\rm W}^{1/2}}\left(\frac{eV}{2l\hbar}\right)^{3/2} = \overline{B_{\rm tunn}}\left(\frac{V}{2l}\right)^{3/2}. \tag{7}$$

Here, $v_{\rm W} = 10^8\,{\rm cm/s}$ is the characteristic velocity of electrons and holes in GLs, and $\overline{B_{\rm tunn}} = [(e/\hbar)^{3/2}/4\pi\, v_{\rm W}^{1/2}] \simeq 5\times 10^{17}\,{\rm s^{-1}\,cm^{-1/2}\,V^{-3/2}}$.

Thus, combining eqs. (5)–(7), we arrive at

$$D^* = \frac{K^*\beta}{\hbar\Omega\sqrt{2K\left[\overline{G_{\rm th}}\exp\left(-\dfrac{\hbar\omega_0}{k_{\rm B}T}\right) + \overline{B_{\rm tunn}}\left(\dfrac{V}{2l}\right)^{3/2}\right]}}. \tag{8}$$

Figure 4 shows the detectivity vs number of GLs calculated in the case of dominant thermogeneration at $T = 300\,{\rm K}$ and in the case that tunneling prevails (curves with markers), which corresponds to relatively low temperatures at $\mathcal{E} = 2.5\,{\rm V/cm}$. As seen from Fig. 4, the detectivity becomes a weak and slightly decreasing function of the number of GLs when this number becomes sufficiently large. The point is that K^* as a function of K saturates at large K, while the contribution of the dark current to the detectivity is proportional to $1/\sqrt{K}$. As a result, the detectivity reaches a maximum at K of about few dozens. Indeed, the function $K^*\beta/\sqrt{K} = [1-(1-\beta)^K]/\sqrt{K} \simeq [1-\exp(-\beta K)]/\sqrt{K}$, and hence D^*, reaches maximum at $K = K_{\max} = 55$ with $K^*\beta/\sqrt{K} \simeq 0.097$. Figure 4 also demonstrates that at sufficiently low electric fields, the

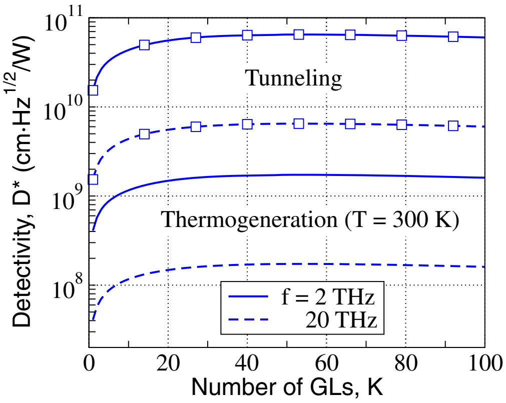

Fig. 4. (Color online) MGL-PD detectivity as a function of number of GLs for different radiation frequencies at $T = 300\,{\rm K}$ (dominant thermogeneration) and at lower temperature (curves with markers) when tunneling is essential.

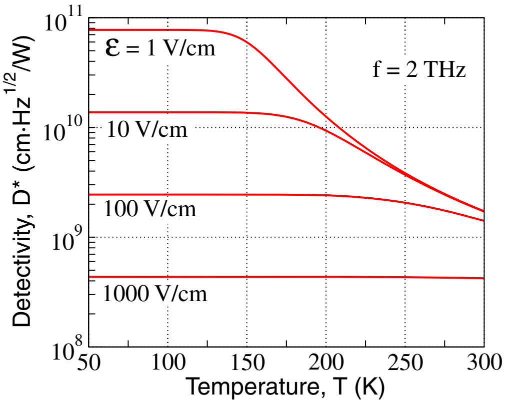

Fig. 5. (Color online) Temperature dependences of MGL-PD detectivity at different electric fields.

detectivity at $T = 300\,{\rm K}$ is mainly limited by the dark current of the thermogeneration origin. Figure 5 shows the temperature dependences of the detectivity of an MGL-PD with $K = 50$ and $K^* \simeq 30$ calculated using eq. (8) for different values of the electric field $\mathcal{E} = V/2l$. The fact that at elevated temperatures (room temperatures and lower), the detectivity is mainly limited by the dark current is confirmed by the comparison of the detectivity temperature dependences at $\mathcal{E} = 1$ and $10\,{\rm V/cm}$ shown in Fig. 5. As seen, the detectivity is virtually independent of $\mathcal{E}$ in the interval $\mathcal{E} = 1$–$10\,{\rm V/cm}$ in the temperature range $T = 200$–$300\,{\rm K}$. It also follows from Fig. 5 that at $T = 100\,{\rm K}$ and sufficiently low electric field, the detectivity can be fairly high. This conclusion can also be drawn from Figs. 6 and 7, where we demonstrate the dependences of the MGL-PD detectivity on the electric field in the i-section at $f = 2$ and $10\,{\rm THz}$.

4. Limitations of MGL-PD Model

Above, we disregarded the recombination of electrons and holes in the i-section under the assumption that the length of this section is not very large. Such an assump-

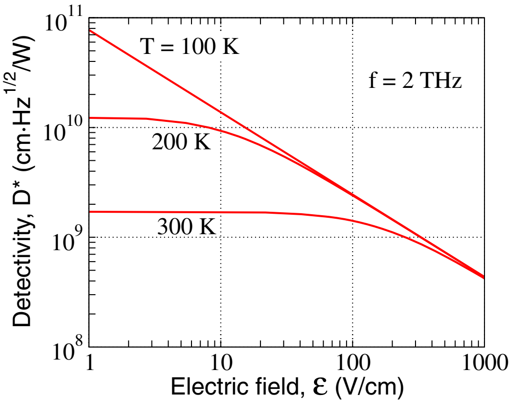

Fig. 6. (Color online) MGL-PD detectivity as a function of the electric field at different temperatures ($f = 2$ THz).

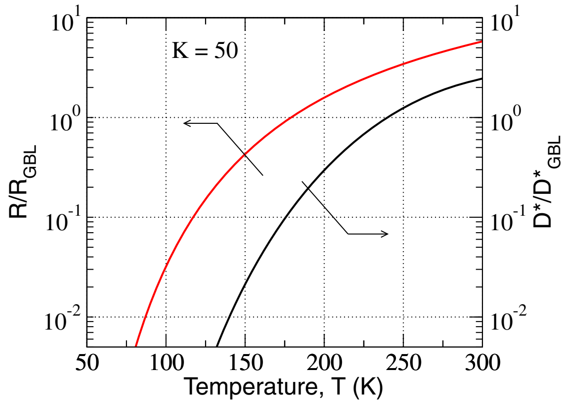

Fig. 8. (Color online) Temperature dependences of the ratios of the responsivities and detectivities of MGL-PDs and GBL-PTs.

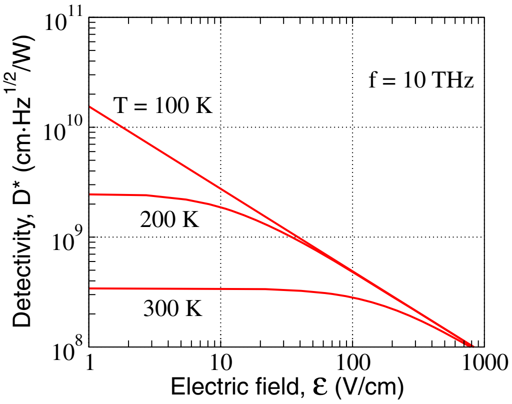

Fig. 7. (Color online) The same as in Fig. 6 but for $f = 10$ THz.

tion implies that the electron and hole transit time across the i-section τ_{trans} is shorter than the characteristic recombination time τ_r. Otherwise, $g < 1$, that reduces the responsivity and detectivity. In the case of collision-dominated transport, $\tau_{trans} = 2l/\mu\mathcal{E}$, where μ is the electron and hole mobility in the i-section. This leads to the following condition:

$$2l < \mu\mathcal{E}\tau_r = l_r. \tag{9}$$

As follows from Figs. 6 and 7, the room-temperature detectivity as a function of the electric field saturates at $\mathcal{E} \lesssim 100$ V/cm. Considering this and setting $\mu = (1\text{–}2) \times 10^4\,\mathrm{cm^2\,V^{-1}\,s^{-1}}$ and $\tau_r = 10^{-10}$ s, we find that the characteristic recombination length $l_r \simeq (1\text{–}2)$ µm. Such a length is markedly smaller than the THz radiation wavelength $\lambda = c/f$, that can result in the problems with the radiation coupling associated with diffraction.[15] Thus, one needs either to increase the electric field (the bias voltage), sacrificing the detectivity value, or to use a special antenna or grating for the effective coupling of radiation. At lower temperatures and higher mobilities, the situation becomes easier. Indeed, at $T \lesssim 150$ K, setting $\mathcal{E} = 100$ V/cm, $\mu = (5\text{–}20) \times 10^4\,\mathrm{cm^2\,V^{-1}\,s^{-1}}$, and $\tau_r = 10^{-9}$ s, we obtain $l_r \simeq 50\text{–}200$ µm, whereas for $f = 2\text{–}10$ THz, $\lambda = 30\text{–}150$ µm.

5. Comparison of MGL-PDs with GBL-PTs

As proposed previously,[8,10] GNR arrays and GBLs can also be used in the phototransistor structures, GNR- and GBL-PTs, for high-performance THz and IR detection. The quantum efficiency of interband transitions in GNR- and GBL-PTs is moderate if they comprise a not very dense GNR array or a single GBL. However, the GNR- and GBL-PTs can exhibit large photoelectric gains due to the long lifetime of photogenerated holes accumulated under the FET gate. It is interesting to compare the responsivity and detectivity of MGL-PDs with those of GBL-PTs. The structure of a GBL-PT is shown in Fig. 2(c). It is assumed that the positive and negative voltages, $V_b > 0$ and $V_t < 0$, are applied to the back and top gates, respectively. In contrast to MGL-PDs, GBL-PTs are sensitive to radiation with the photon energy $\hbar\Omega$ exceeding the energy gap E_g induced by the gate voltages.

As follows from ref. 10, at $\hbar\Omega \gtrsim E_g$, the photoelectric gain in GBL-PTs can be estimated as

$$g_{GBL} \sim \exp\left(\frac{0.65\varepsilon_F}{k_B T}\right), \tag{10}$$

where ε_F is the Fermi energy in the source contact. Taking into account that the photoelectric gain in MGL-PDs is $g \simeq 1$ and neglecting the interband tunneling in GBL-PTs, for the ratios of R/R_{GBL} and D^*/D^*_{GBL}, we obtain

$$\frac{R}{R_{GBL}} \simeq 2K^* \exp\left(-\frac{0.65\varepsilon_F}{k_B T}\right), \tag{11}$$

$$\frac{D}{D^*_{GBL}} \simeq \frac{2K^*}{\sqrt{K}} \exp\left(-\frac{0.325\varepsilon_F}{k_B T}\right) \times \sqrt{\frac{\overline{G_{th}} \exp\left(-\dfrac{\hbar\omega_0}{k_B T}\right)}{\overline{G_{th}} \exp\left(-\dfrac{\hbar\omega_0}{k_B T}\right) + \overline{B_{tunn}}\left(\dfrac{V}{2l}\right)^{3/2}}}. \tag{12}$$

Figure 8 shows the temperature dependences of R/R_{GBL} and D^*/D^*_{GBL} calculated using eqs. (11) and (12). It was assumed that the Fermi energy $\varepsilon_F = 100$ meV, $K = 50$, $K^* = 39$, and $\mathcal{E} = 100$ V/cm. One can see from Fig. 8 that at elevated temperatures, the MGL-PD responsivity (at $T \gtrsim 180\,\mathrm{K}$) and detectivity (at $T \gtrsim 240\,\mathrm{K}$) exceed those of GBL-PTs. However, at lower temperatures, the situation reverses. This is attributed to a dramatic increase in the photoelectric gain in GBL-PTs with decreasing temperature.

6. MGL-PDs vs Other THz and IR Detectors

The detection of THz and far-IR radiation can, in principle, be realized using the interband transition in the structures with bulk semiconductors, such as HgCdTe (MCT), with sufficiently narrow energy gap.[16] Leaving aside the fabrication problems, let us compare MGL- and MCT-PDs. The absorption coefficients in these detectors can be close to unity, so that both of them exhibit similar quantum efficiencies. However, MGL-PDs can exhibit a lower thermoexcitation rate, the factor crucially affecting the detectivity. This is because the energy of optical phonons $\hbar\omega_0 \simeq 0.2\,\mathrm{eV}$ in GLs is much larger than that in MCT. As a result, even at room temperature, the number of optical phonons $N_0 \simeq \exp(-\hbar\omega_0/k_BT) \ll 1$. Because of this, the thermogeneration associated with the absorption of optical phonons in GLs is relatively weak. Another mechanism that could contribute to the thermogeneration in GLs is the absorption of acoustic phonons. However, owing to the low velocity of acoustic waves s in comparison with the characteristic velocity of electrons and holes in GLs, $v_W = 10^8\,\mathrm{cm/s}$, the one-phonon interband absorption is forbidden. The Auger processes, which are fairly strong in MCT, are also forbidden[22] in GLs because of the linear symmetric dispersion relation for electrons and holes. Thus, one can expect that MGL-PDs can markedly surpass NCT-PDs in the dark-current detectivity.

Further development of quantum-well intersubband photodetectors (QWIPs) and quantum-dot intersubband photodetectors (QDIPs) has also resulted in the possibility of THz and far-IR detection with these devices.[23] However, the absorption coefficients in a QW and a QD array are about one order of magnitude smaller than that in a GL ($\beta_{QW} \sim 0.002$). The photoionization energy of electrons (or holes) in QWs and QDs ε_i should be sufficiently small to provide the condition $\hbar\Omega \gtrsim \varepsilon_i$. Due to a smallness of ε_i, the thermoexcitation rate in QWIPs and QDIPs appears to be much higher than in MGL-PDs. Apart from this, the tunneling from QWs and QDs can also greatly contribute to the dark current and thus worsen the QWIP/QDIP performance.

One of the noteworthy features of MGL-PDs is that their detectivity decreases with increasing radiation frequency (compare Figs. 6 and 7), whereas other detectors usually exhibit increasing dependences.

7. Conclusions

We calculated the responsivity and dark-current-limited detectivity of MGL-PDs as THz and IR detectors. As shown, the interband tunneling can be an essential mechanism behind the dark current and, hence, the MGL-PD detectivity at low temperatures. This mechanism limits the ultimate values of detectivity and necessitates the optimization of the device structure and proper choice of the temperature and bias voltage. We show that, owing to the high values of quantum efficiency and the relatively low rates of thermogeneration, the detectors under consideration can exhibit high responsivity and detectivity at elevated temperatures, in particular, at room temperature, in a wide radiation spectrum and can substantially surpass other detectors, for instance, GBL-PTs, QWIPs, and QDIPs. Thus, MGL-PDs appears to have considerable promise as high-temperature wide-band (or multicolor) THz and IR detectors.

Acknowledgment

The authors are grateful to Dr. C. Berger for useful discussion and critical comments during the presentation of this work at ISGD 2010. The work was supported by CREST, the Japan Science and Technology Agency.

1) A. H. Castro Neto, F. Guinea, N. M. R. Peres, K. S. Novoselov, and A. K. Geim: Rev. Mod. Phys. **81** (2009) 109.
2) L. A. Falkovsky and A. A. Varlamov: Eur. Phys. J. B **56** (2007) 281.
3) N. M. R. Peres, F. Guinea, and A. H. Castro Neto: Phys. Rev. B **73** (2006) 125411.
4) V. Ryzhii, M. Ryzhii, and T. Otsuji: J. Appl. Phys. **101** (2007) 083114.
5) F. Rana: IEEE Trans. Nanotechnol. **7** (2008) 91.
6) A. Dubinov, V. Ya. Aleskin, M. Ryzhii, T. Otsuji, and V. Ryzhii: Appl. Phys. Express **2** (2009) 092301.
7) V. Ryzhii, M. Ryzhii, V. Mitin, and M. S. Shur: Appl. Phys. Express **2** (2009) 034503.
8) V. Ryzhii, V. Mitin, M. Ryzhii, N. Ryabova, and T. Otsuji: Appl. Phys. Express **1** (2008) 063002.
9) F. Xia, T. Murller, Y.-M. Lin, A. Valdes-Garsia, and F. Avouris: Nat. Nanotechnol. **4** (2009) 839.
10) V. Ryzhii and M. Ryzhii: Phys. Rev. B **79** (2009) 245311.
11) M. Sprinkle, D. Suegel, Y. Hu, J. Hicks, A. Tejeda, A. Taleb-Ibrahimi, P. Le Fevre, F. Bertran, S. Vizzini, H. Enriquez, S. Chiang, P. Soukiassian, C. Berger, W. A. de Heer, A. Lanzara, and E. H. Conrad: Phys. Rev. Lett. **103** (2009) 226803.
12) M. Orlita and M. Potemski: Semicond. Sci. Technol. **25** (2010) 063001.
13) V. Ryzhii, M. Ryzhii, A. Satou, T. Otsuji, A. A. Dubinov, and V. Ya. Aleshkin: J. Appl. Phys. **106** (2009) 084507.
14) V. Ryzhii, A. A. Dubinov, T. Otsuji, V. Mitin, and M. S. Shur: J. Appl. Phys. **107** (2010) 054505.
15) V. Ryzhii, M. Ryzhii, V. Mitin, and T. Otsuji: J. Appl. Phys. **107** (2010) 054512.
16) A. Rogalski, J. Antoszewski, and L. Faraone: J. Appl. Phys. **105** (2009) 091101.
17) D. Farmer, Y.-M. Lin, A. Afzali-Ardakani, and P. Avouris: Appl. Phys. Lett. **94** (2009) 213106.
18) V. V. Cheianov and V. I. Fal'ko: Phys. Rev. B **74** (2006) 041403(R).
19) M. Ryzhii, V. Ryzhii, V. Mitin, T. Otsuji, and M. S. Shur: Phys. Rev. B **82** (2010) 075419.
20) A. Rose: *Concepts in Photoconductivity and Allied Problems* (Wiley, New York, 1963).
21) F. Rana, P. A. George, J. H. Strait, S. Shivaraman, M. Chanrashekhar, and M. G. Spencer: Phys. Rev. B **79** (2009) 115447.
22) M. S. Foster and I. L. Aleiner: Phys. Rev. B **79** (2009) 085415.
23) H. Luo, H. C. Liu, C. Y. Song, and Z. R. Wasilevski: Appl. Phys. Lett. **86** (2005) 231103.

Maxim Ryzhii obtained MS degree from Moscow Institute of Physics and Technology, Russia, in 1992. In 2001, he obtained Doctor of Engineering degree from Tokyo Institute of Technology, Japan. From 1993, he has been with the University of Aizu, Japan, where he is now an Assistant Professor at Computational Nanoelectronics Laboratory. His research activity is associated with physics and computer modelling of low-dimensional semiconductor heterostructures and devices, including electron and optotoelectron devices based on nanostructures. He is an author and co-author of more than 60 journal publications and numerous conference papers. Dr. M. Ryzhii is a Senior Member of the Institute of Electrical and Electronics Engineers.

Taiichi Otsuji received the B.S. and M.S. degrees in electronic engineering from Kyushu Institute of Technology, Fukuoka, Japan, in 1982 and 1984, respectively, and the Dr. Eng. degree in electronic engineering from Tokyo Institute of Technology, Tokyo, Japan in 1994. From 1984 to 1999 he worked for NTT Laboratories, Kanagawa, Japan. In 1999 he joined Kyushu Institute of Technology as an associate professor. Since 2005 he has been a professor at the Research Institute of Electrical Communication, Tohoku University, Sendai, Japan. His current research interests include terahertz electronic and photonic devices and their applications. He is the recipient of the Outstanding Paper Award of the 1997 IEEE GaAs IN Symposium. He is a member of the Japan Society of Applied Physics, Institute of Electronics, Information, and Communication Engineers, and Institute of Electric and Electronics Engineers, and a Senior member of the Optical Society of America.

Vladimir Mitin is currently SUNY Distinguished Professor at the Department of Electrical Engineering at the University at Buffalo, the State University of New York. He obtained his Ph. D. and Doctor of Science degrees from the Institute of Semiconductors of Ukrainian Academy of Sciences, Kiev, in 1971 and 1987, respectively. His fields of specialization are nanoelectronic, microelectronic and optoelectronic devices and materials with special emphasis on sensors and detectors based on nanostructures. He has more than 500 publications including ten patents, four monographs and five textbooks. Vladimir Mitin is Fellow of the Institute of Electrical and Electronics Engineers, American Association for Advancement of Science, and the Institute of Physics.

Victor Ryzhii has been a Professor of the University of Aizu, Japan, since 1993. He obtained his Ph. D. and Doctor of Science degrees from Moscow Institute of Physics and Technology, Russia, in 1970 and 1975, respectively. His research activity is associated with physics and computer modelling of low-dimensional semiconductor heterostructures and electron, optotoelectron, and terahertz devices based on nanostructures, including graphene-based devices. He has about 300 journal publications, numerous conference papers, and 11 patents. Victor Ryzhii is Fellow of the Institute of Electrical and Electronics Engineers, Fellow of the American Physical Society, Corresponding Member of the Russian Academy of Sciences, and a member of the Japan Society of Applied Physics.